CU Boulder Wind Team
2023-2024

Turbine Design Final Report

April 18th, 2024

Student Lead:

Elyse DeBarros
Elyse.DeBarros@colorado.edu

Kaity Plutt – *Turbine Design and Testing Lead*
Aria Mundy – *Financial Manager*
Carver Lindley – *CAD Engineer*
Dane Robinson – *Electromechanical Engineer*
Donggyu Jang – *Turbine and Wind Farm Engineer*
Liam West – *CC Lead & Turbine Engineer*
Loren Peterson – *Electromechanical Lead*
Megan Finnigan – *Test Engineer*
Preston Brumley – *Controls Engineer*
Stewart Rojec – *Electrical Engineer*
Tim Herwig – *Logistics Manager*

Faculty Advisor:

Roark Lanning
Roark.Lanning@colorado.edu

Table of Contents

Executive Summary

As part of the 2024 Collegiate Wind Competition (CWC) sponsored by the Department of Energy and the National Renewable Energy Laboratory, this year's CU Boulder Wind Team has designed a small-scale prototype offshore wind turbine capable of withstanding wind speeds up to 22 m/s. The turbine will compete in a set of six tasks to evaluate its performance in conditions that model real-world scenarios and will be scored based on its ability to function safely and reliably while fulfilling requirements put forth by the CWC. This report details the technical design of this wind turbine, including the design goals, mechanical loading analysis, aerodynamics, electrical design, software architecture, and testing progress made by the team.

Figure 1. Full turbine assembly and CAD model

This year's turbine utilizes a suction caisson as the anchoring system. The stub piece will slide smoothly over the top tube of the foundation. A ¼-inch base plate serves as an interface between the stub piece and tower, which is held in place by a collar placed on the exterior of the aluminum tube. This year's team opted to use manual yaw, which features a yaw collar connected to the nacelle base plate and is aligned by hand with the prominent wind direction, held in place with two set screws. The nacelle includes a mechanical brake fashioned after a bicycle disc brake, the generator, the drive shaft and its supports, and a place to ground the base plate. A new triple Miter gear pitching system has been implemented with a custom-made clamshell gearbox to house the gears and blade shafts, which hold the blades in place and are secured with shoulder bolts. The pitching system is powered by a Pololu gearmotor and uses a slip ring to transmit signals and power to the rotating motor. A main drive shaft transfers power from the mechanical power in the wind harnessed by the blades to the generator.

The electrical system consists of one PCB on each side of the Point of Common Coupling (PCC). A brushless DC motor is used as the generator, which powers each turbine side system. The turbine's primary load is a MOSFET and a sense resistor for feedback current control. The load PCB also houses an Arduino Uno microcontroller, which sends optocoupled signals for pitching, braking, and load control while receiving information about rotor speed, motor positioning, and power.

Design Overview
Design Objective

The fourth University of Colorado Collegiate Wind Competition team's goal was to design, manufacture and test a small-scale offshore wind turbine that will perform safely and efficiently during the turbine testing competition tasks. The 22-23 CU CWC team performed well in the durability,

foundation success and foundation weight tasks, but struggled to earn points in the power curve and control of rated power and rotor speed tasks. For this reason, our team's focus has centered around improving the pitching, electrical, and controls systems, to convey signals more reliably and mitigate problems that last year's team experienced. We also focused on simplifying our emergency stop system for reliability and repeatability.

Components from Prior Competition

There are two design aspects from last year's turbine that were analyzed, tested, and proven to be the best option to meet the team's design goals. They include the following components:

Suction Caisson Foundation

The team's suction caisson design earned 88 of a possible 90 points in last year's CWC for the foundation success and foundation weight tasks. The 2024 CU CWC team conducted calculations to further optimize the size of the suction caisson. We considered passive and active earth pressures and suction forces to counter the overturning moment from nacelle drag and thrust and drag on the blades. We manufactured and tested a new suction caisson without last year's height adjustment piece. Additionally, the team conducted testing with the foundation system to ensure it could sustain the maximum theoretical expected forces. These results are discussed in more detail below.

Maxon 488607 Generator

The team evaluated 8 generators. They were first compared in a MATLAB model that used generator specifications to predict the efficiency of power generation. The two top-performing generators from the model were then compared in physical testing (further explained below). The Maxon EC-i40 488607 generator was chosen based on its performance in both theoretical modelling and physical testing.

Changes from Prior Competition

New design changes include a complete overhaul of the pitching system to include a triple Miter gear assembly inspired by the Cal Maritime design from 2023, removal of the height adjustment piece from the foundation assembly, a modification to the base collar so it surrounds the exterior of the tower tube, the implementation of a manual yaw system, a redesign of the mechanical brake fashioned after a bicycle disc brake, a complete redesign of the turbine and load electrical systems, and a modified control scheme.

Static Performance Analysis

The turbine blades must capture the maximum amount of energy in the wind during the power curve task, while remaining lightweight and fitting within the designated tolerances. The angle of twist of the blade was optimized to enable power production at low wind speeds, and a literature review advised a Tip Speed Ratio (TSR) of 7 [1].

The majority of the team's blade optimization and calculations were conducted in QBlade, a simulation software that analyzes wind turbine blade performance and aerodynamics in a variety of conditions. QBlade's algorithms are based on the Blade Element Momentum (BEM) Theory, which is central to proper blade analysis.

The preliminary design process for the turbine blade's airfoils considered benchmarking other teams, and optimizing airfoils based on their glide ratio (C_L/C_d) at relevant Reynolds numbers (between 60,000-265,000) as well as maximizing thickness as a percent, to at least 10% of the chord length. Airfoils were selected from the Airfoil Tools Database. In QBlade, the blade cord lengths and twist angles were optimized with the Betz law and our selected TSR (lambda). We chose the SG 6042 air foil. We designed multiple blades with a TSR of 4 and 7, which perform best in the literature [1]. We plan to test which TSR will be the most optimal in the weeks before competition, using the UCAR Wind Tunnel discussed in the Testing section.
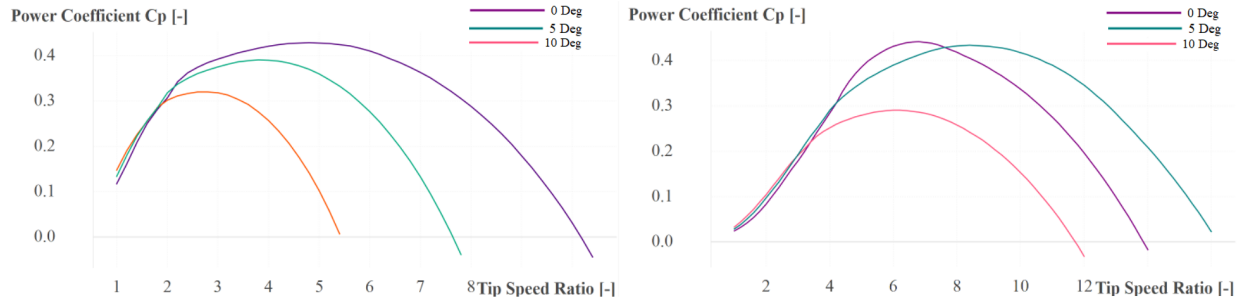
Figure 2. A graph showing the Coefficient of Power (Cp) vs Tip Speed Ratio at 8 m/s. Optimization for TSR 4 (left) and TSR 7 (right).

The max coefficient of power (C_p) QBlade anticipates is 0.43 for the blade design optimized at a TSR of 7, shown on the right, and 0.43 for design optimized at TSR 4, shown on the left. Both values are less than the Betz limit of 0.593. The use of Qblade's Prandtl Tip Loss and 3D Correction adjusted the solutions to be more accurate and put them in a range we expect to see in testing.

Annual Energy Generation

Using the 2012 wind speed data from the Wind Toolkit for Boulder, Colorado with an adjusted a hub height of 95 cm (as mandated by competition specifications), the annual energy generation was estimated to be 35.4 MWh, assuming a blade length of 22.5 cm. This is enough energy to supply a house with electricity for 42.5 months, power 71 refrigerators nonstop for a year, or drive an electric car 127,440 miles [2].

Engineering Diagrams of Mechanical Systems & Load Analysis

Emergency Stop

A modified braking mechanism will allow the turbine to perform better during the emergency stop task. Last year's design featured a triple redundancy emergency stop system that employed a mechanical brake, shorting the generator, and negative pitching. This year's turbine utilizes a simple mechanical brake inspired by a disc brake on a bicycle. The system consists of a custom disc rotor mounted to the back-shaft of the generator, and a custom brake caliper assembly with off-the-shelf bike brake pads. We are using a linear actuator with a 1:375 gear ratio to deliver a pushing force of 200 N to the generator. We calculated the maximum possible braking force using common friction coefficients of off-the-shelf bike brake pads and the given actuator force. Multiplying by the radius of the rotor gives us a braking torque of 3.18 N-m. We then considered the overall moment of inertia of all rotor and driveshaft components and found that this e-brake design could decelerate from 2800 RPM to 0 RPM in about 0.5 seconds, 20 times faster than the required 10 seconds.
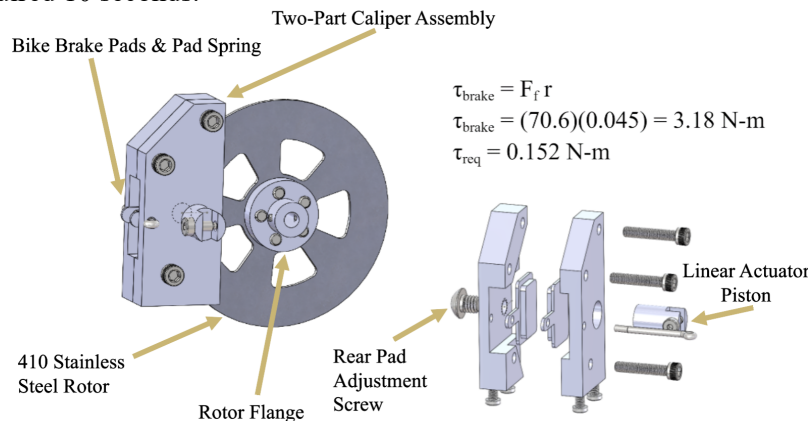

$$\tau_{brake} = F_f\, r$$
$$\tau_{brake} = (70.6)(0.045) = 3.18 \text{ N-m}$$
$$\tau_{req} = 0.152 \text{ N-m}$$

Figure 3. Emergency stop design and factor of safety calculations.

4

Pitching System

      To improve our performance in the power curve and control of rated power and rotor speed tasks, we redesigned the turbine's pitching system from a swash plate design to a miter gearbox design. Our miter gearbox redesign features a robust system that can accurately pitch with minimal power draw and reduces the risk of binding by eliminating all metal-on-metal sliding interfaces. It utilizes a 6V DC 499:1 gearmotor that is mounted directly to the driveshaft inside a hollow aluminum housing component. An integrated 48 CPR quadrature encoder sends signals back to the Arduino which uses proportional feedback to control the angular position of the gearmotor's output shaft.
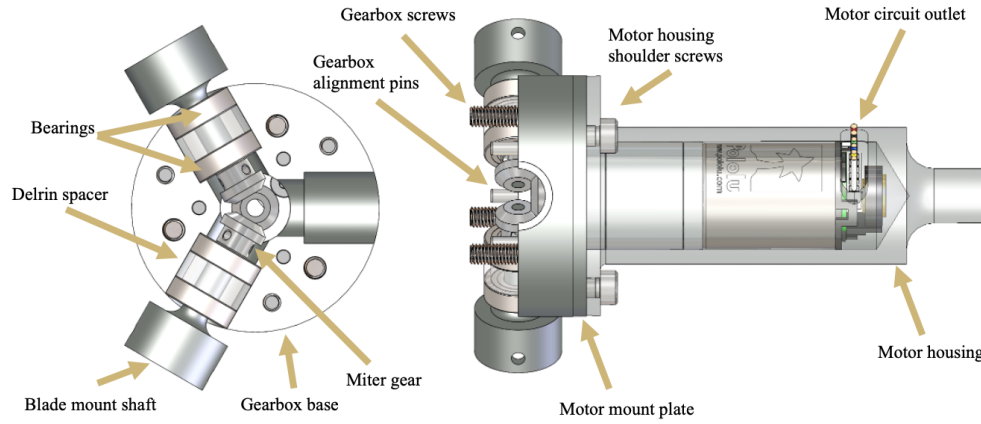

Figure 4. Internals of the miter gearbox pitching assembly

      A central drive gear is mounted directly to the gearmotor shaft and meshes with the 3 blade gears with a 1:1 ratio. Each blade gear is attached to a blade mount shaft, which means that 1 degree of angular actuation of the drive gear corresponds to 1 degree of blade pitch. Equation 1 was used to determine the anticipated maximum torque each blade would experience. We assumed a windspeed of $U_\infty = 22$ m/s, a rotational velocity of $\omega = 2800$ rpm, and used a moment coefficient pulled from QBlade of $C_m = 0.15$. The blade torque was then multiplied by 3 to find the max torque on the drive gear to be 0.15 N-m. The chosen gearmotor is rated to provide torque up to 0.49 N-m.

$$T_{blade} = \frac{C_m \rho}{2} \int_0^R (U_\infty^2 + (r\omega)^2) * L_c^2 dr$$

      1

      Our miter gear selection was informed by using a modified Lewis equation, shown in Eq.2, and the previously calculated max torque value of 0.15 N-m. We decided to use a 10 mm pitch diameter, 20 tooth, 20° pressure angle, 1045 steel gear manufactured by Misumi. We used a conservative tensile yield strength of 310 MPa for the 1045 steel material (typical range of 310-450 MPa).

$$\sigma_{tooth} = \frac{2T_p}{dFmJ} * \frac{K_a K_m K_s}{K_v K_x}$$

      2

      Even under the most extreme anticipated shock loading scenarios, this gear will theoretically hold a tooth shear safety factor of 3.9. The gearbox itself is a clamshell design machined from 7075-T6 Aluminum, which allows us to open it entirely for any assembly, adjustments, or maintenance, while still being stiff enough to hold the precise miter gear mesh in place even under maximum stress conditions.
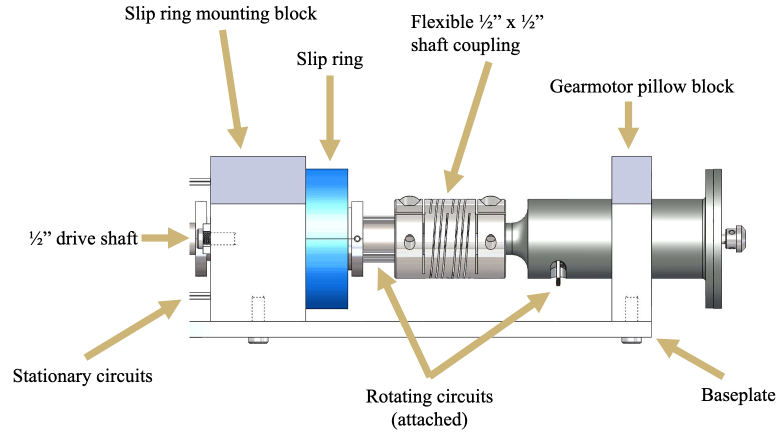
Figure 5 Rotor drive shaft layout.

Since the gearmotor itself is spinning with the rotor, we utilized a high-speed through-bore slip ring, rated for continual use up to 5000 RPM, that allows us to send power and signal between the gearmotor and the Turbine PCB. However, during testing we discovered that the slip ring adversely affects the signal quality from the pitching encoder, and we decided to include a Schmitt trigger on the Load PCB to ensure clean, crisp square waves are reaching the Arduino.

Blade and Rotor Analysis

Beyond the optimization of the blades' power output, we needed to ensure their structural integrity. Figure 6 shows the free body diagram for all forces acting on the spinning blade using simplified Blade Element Momentum theory [3]. This analysis was conducted in three dimensions using cylindrical coordinates. The forces acting on the blade include centripetal, drag, lift and acceleration from emergency stop. It also includes internal reaction forces acting on the root of the blade (reactions forces were solved in 3d but only 1d is shown in Figure 6 for clarity). The internal reactions include shear (V), normal (N) and bending/moment (M). A MATLAB model was created to calculate all forces on the blade root, assuming a rotational velocity of 2800 RPM and an emergency stop deceleration of 3.18 N-m.
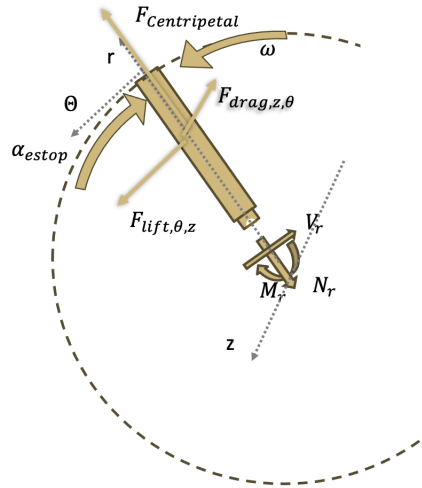

Figure 6. A free body diagram of one blade for structural analysis.

The failure modes we were concerned about were bending failure at the root of blade and through-hole tear-out. Our analysis considered stress concentrations from the through hole in the blade root, using

the Peterson stress concentration charts [3]. The model we created was parameterized first for the diameter of the blade root. We also explored using two different 3D printed materials. Next, we parameterized for the mounting through hole considering the associated stress concentration.
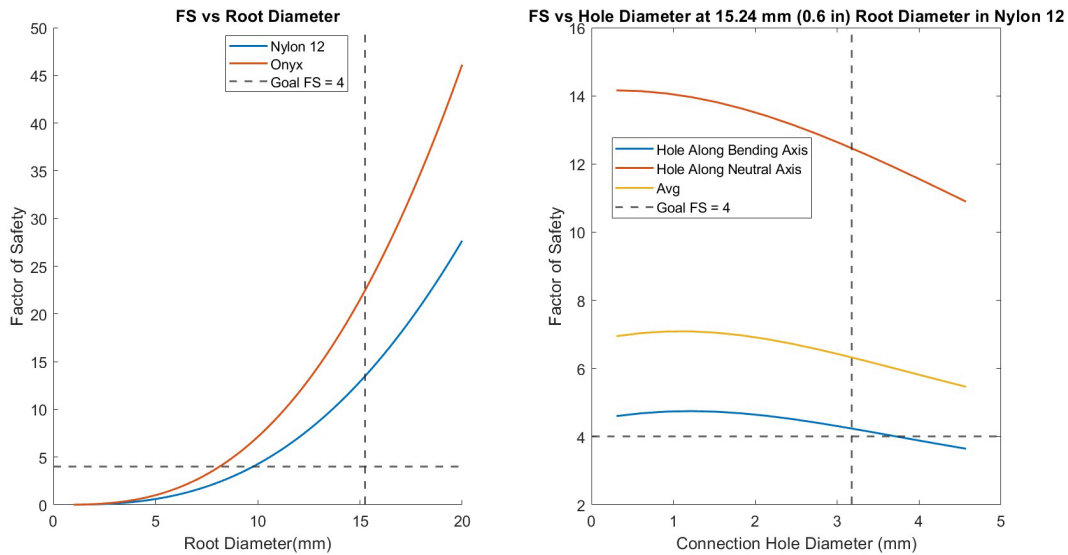

Figure 7. (Left) Blade root diameter vs factor of safety. (Right) Assuming chosen root diameter from right, parametrized for through hole diameter and through hole orientation.

The blade root is one of the failure points we are most concerned about, and it is difficult to precisely model the loading conditions a blade will undergo during testing. For this reason, we chose to design the blade root with a conservative factor of safety (FS) of 4. We chose to manufacture the blades by 3d printing them in Nylon 12 using a FormLabs Fuse1 SLS printer (blue on the left in Figure 7). While Nylon 12 has a smaller ultimate yeild strength than ONYX, an SLS print is perferable over an FDM print because FDM prints introduce anisntropic materials propeties that would be undesirable. We decided we were able to compensate for the weaker material with a thicker diamter section. We chose a diameter of 15.24mm for the blade root and a 3.98mm (5/32") through hole for connecting to the rotor.

We translated the load calculations from the blades into an analysis of the connection shaft (blade shaft) between the blade and pitching system.
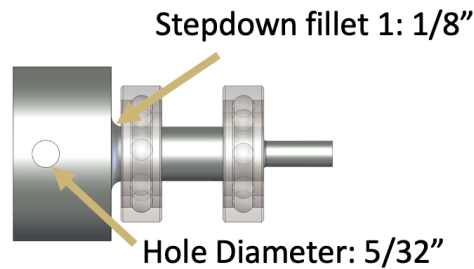

Figure 8. Blade shaft key dimensions.

We were concerned about hole tear out and failure at each of the two steps of this component due to stress concentrations. We integrated this analysis into the MATLAB model mentioned above and designed the connection within similarly conservative safety factors: hole tear out FS: 4.25, failure at stepdown 1 FS: 4.75, failure at stepdown 2 FS: 15.15.

Nacelle and Yaw Sub-System

The yaw system must align the turbine rotor with the predominant wind direction, despite the bolt orientation of the stub piece being unknown. Installation must be quick and provide stable alignment throughout turbine testing. This year's team chose to use a simple yaw collar with two set screws to manually align the nacelle with the wind direction. A mechanical analysis is shown below, assuming a maximum of a 5-degree misalignment with the wind direction from visual inspection.

When deciding on a manual yaw system, we were first concerned with potential power losses from misalignment. We explored the equation for the power generated by a wind turbine. If the turbine can only harness the fraction of wind energy perpendicular to the swept area, swept area A would be replaced by the projection of the swept area when there is a yaw misalignment of angle θ. This projection is an ellipse with an area of A*cos(θ). Then, the power equation is given by:

$$P = \frac{1}{2} C_p \rho A v^3$$

We can expect that the actual power produced from misalignment could be less than the expected value because our airfoils will no longer behave ideally. However, at a small misalignment, the non-idealities would be small, and the equation above should be valid. Therefore, the expected power output from a 5° misalignment would be about 99.6%, meaning we expect less than 1% power loss.

Secondly, we needed to ensure the yaw setscrews would be able to withstand uneven loading due to potential maximum 5° misalignment. We simplified the distributed loadings on the blades from the wind to point loads at the tips and neglected the forces on the nacelle. We used the blade loading MATLAB model mentioned above, assuming a wind speed of 22 m/s, and found the maximum force in the downwind direction to be a distributed load of 24 N across the blades, increasing towards the outer tip.
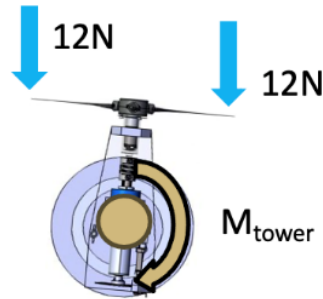

Figure 9. A top-down free body diagram of the turbine and the forces on the blades with a 5° misalignment.

At a 5° misalignment, the difference in the moment arm from the center of the tower is 0.044 m. The torque would be 0.06 N*m. We decided to use ¼" 20 hex head cone head set screws to lock the yaw collar rotation on the tower. Based on tabulated results from safety socket [4]. we found that a ¼" diameter set screw can give us a holding torque of 85 N-m. The FS for torque on yaw is 2833.

Tower Design

The turbine tower is responsible for supporting the weight of the nacelle and rotor subassemblies as well as any nacelle drag and thrust from the rotor. We wanted to check buckling and bending failure. A moment due to a maximum misalignment in the yaw system of 5 degrees was also included in calculations, as shown below.
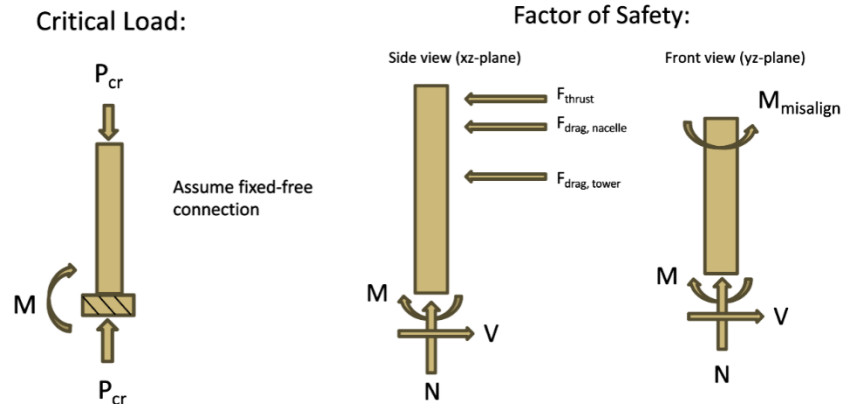
*Figure **10**. Static analyses of the tower.*

Based on these calculations, it would require 24,500 N of force to cause buckling in the tower tube, which is much greater than the expected load of 44.5 N from the weight of the nacelle and rotor assemblies. The expected shear force caused by thrust and drag forces is 23.3 N. Combining the effects of the vertical weight forces of the rotor and nacelle and the horizontal forces from thrust, the net stress is 4.702 kPa. Comparing this with a yield strength of 265 MPa for Aluminum 6061-T6 gives a very comfortable safety factor of about 50.

The team modified the tower base collar and yaw mechanism so that both lie on the exterior of the tower to allow for a minimum of 1 inch of clearance for electrical connectors.

Foundation Engineering Diagram

The foundation must provide stable anchorage for the turbine, remain within dimensional limitations, and comply with the no-excavation rule. Per competition requirements, it must also withstand rotor forces at wind speeds up to 22 m/s. Calculations based on QBlade outputs quantify the horizontal force at the rotor height to be 36 N, which applies a moment of 34.2 N-m on the foundation. Several foundation designs were considered to meet these requirements. As mentioned in the prior competition section, we chose a suction caisson as the final design because it is lightweight, easy to install, and strong enough to meet the functional requirements, as discussed below.

We conducted a civil engineering analysis to assess the stability of the suction caisson design in the context of varying earth pressures. Research showed that this analysis could focus solely on evaluating the passive earth pressure's impact on the rotating bucket's stability, with negligible consideration for active and at-rest earth pressures [5]. This simplified approach involved defining passive earth pressures using specific equations accounting for lateral and vertical stresses applied to the caisson, as shown in Figure 11. Moreover, a static analysis was performed to ensure that soil and suction forces could effectively counteract potential rotation. The resultant forces from these pressures were calculated to confirm that the resisting moment exceeded the overturning moment, considering assumptions regarding force distribution and acting angles. It was assumed that both inner and outer earth pressures act on half of the total bucket surface area either above or below the axis of rotation. Additionally, it was assumed that resultant forces acted in the midplane.

The team developed a MATLAB script to analyze different suction bucket geometries, mainly focusing on different length-to-depth (L/D) ratios of the suction cylinder to identify configurations offering adequate resistance against turbine loads while minimizing weight. The turbine's estimated maximum drag and thrust forces were calculated to be 26.35 N-m, and we decided on designing in a minimum safety factor of 3 to ensure stability against overturning forces. This analysis led to the identification of an optimal design with a diameter of 28.58 cm, a length of 17.17cm, and an L/D ratio of 0.60. The resulting weight of this design, when constructed from 0.813mm thick 4130 steel, totals only 1.39 kg.
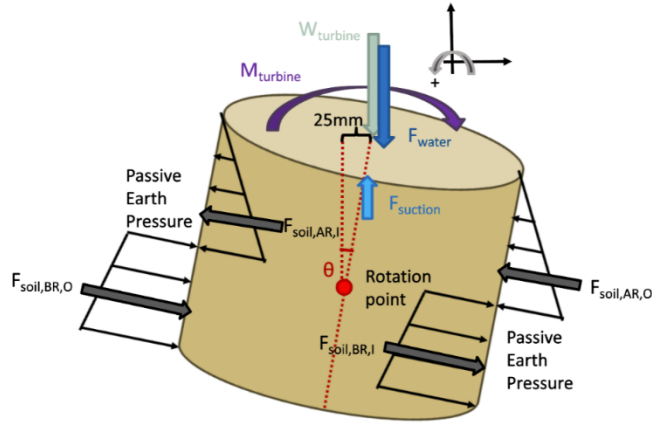
Figure 11. Civil engineering analysis of the suction caisson anchoring system

While the static analysis of this design works out great, the use of such thin sheet metal results in an inherently weak welded connection between the foundation top tube and the suction caisson. To ensure this joint would not fail under maximum stresses, a set of 3 triangular gussets was added to the design, adding strength while contributing negligible additional weight.

Electrical Subsystem

Electrical System Overview and One-Line Diagram

The electrical system is divided into 3 sections to best comply with the competition's isolation requirements. The first is the nacelle, which houses the electronics that need to be physically close to the rotor to operate the turbine. These components include the pitching actuator, brake actuator, and generator. The nacelle also houses a cable assembly that arranges the incoming and outgoing signals and power lines into just 3 connectors for ease of assembly and compliance with competition requirements. The signals transmitted from the nacelle to the next section, the Turbine PCB, are shown in Figure 12.
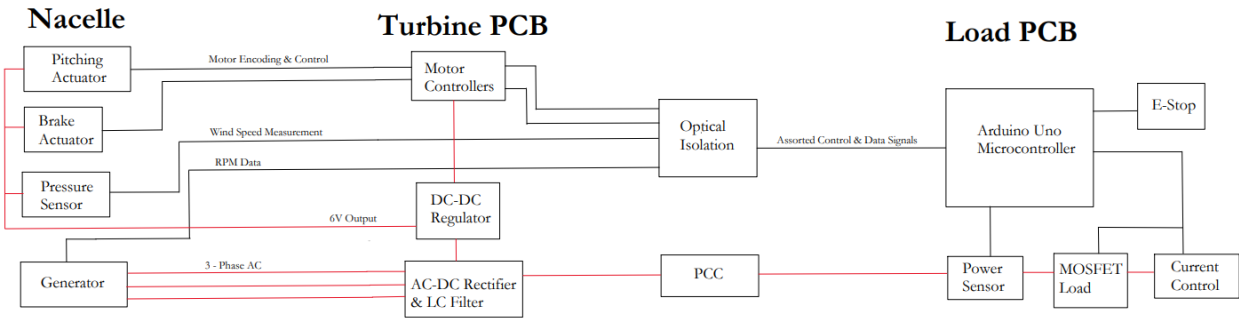

Figure 12. Electrical One-Line Diagram

The Turbine PCB houses turbine power conditioning, a buck-boost converter, pitching & brake motor control, and necessary optical isolation circuitry. Since the entire turbine must be self-powered, active rectification is not possible. Thus, the 3-phase AC power from the generator is rectified using an array of 6 diodes, then filtered using an LC stage before reaching the PCC terminal. To power the nacelle peripherals and the rest of the turbine board, a buck-boost DC-DC converter is connected in parallel with the PCC. Since efficiency is of utmost importance, an off-the-shelf converter is used instead of a custom one. We selected the Pololu S18V20F6 for its wide input range and DC output of 6V, which is within specification to power all the turbine components. The pitching motor is controlled with a Toshiba TB6612FNG motor driver, selected for its versatility and input voltage. The brake control is done with Pulse-Width Modulation from the microcontroller, but still requires some circuitry on this board to ensure

10

functionality. Since the brake must be powered by the turbine, and the brake is used to stop the rotor in an emergency stop condition, energy storage must be added to the turbine board to disengage the brake when to fulfill the automatic restart requirements. To accomplish this, a separate 6V line is used for the brake, and the brake 6V bus includes an 88 mF capacitor bank that can be discharged through a high current gain optocoupler. The other capacitors on the turbine board are a 22 µF decoupling capacitor and the 1 mF filter capacitor. Our total energy storage is calculated below:

$$E = \frac{1}{2}CV^2 = \frac{1}{2}(88 * 10^{-3} * 6.3^2 + 10^{-3} * 50^2 + 22 * 10^{-6} * 10^2) = 2.997 \, J$$

The last section of the electrical design is the Load PCB, which includes our microcontroller, load control circuit, and optical isolation. The microcontroller we selected is an Arduino Uno R3, which is ideal for this application since the control software is relatively simple and not storage intensive, and it has enough GPIO pins to facilitate all necessary communication, including an I²C bus. It is powered by a 12 V input from a wall AC converter, which is also used by the current control circuit, and provides the 5 V bus for the rest of our components. For our load, we decided to use an N-channel enhancement MOSFET because they have a large power dissipation capacity and a highly variable impedance depending on the gate voltage. This gives us higher control over the behavior of the generator, since the resistance at its terminals controls the torque required to spin the rotor. The MOSFET is combined in series with a current sense resistor, whose voltage drop can be compared to a reference input from the microcontroller with an op-amp. This allows us to precisely control the current through the load and algorithmically maximize the generator's power output. Increasing the current through the load beyond the maximum power point will also decrease the generator's produced voltage, allowing us to constrain the power line to be within 0-32 V, which is our circuit's designed operating range.
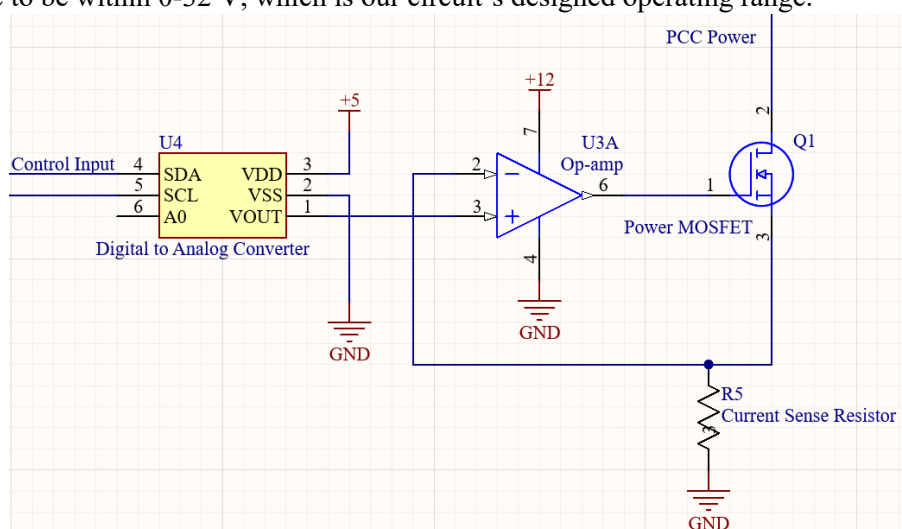

Figure 13. Load Control Circuit Schematic

Signals are optically isolated throughout the electrical system to comply with competition requirements. We used an active high topology for our optocouplers, which means the signals are isolated on the side of the PCC where they're received. The load board receives the generator's Hall sensor and pitching encoder signals, and sends pitching control, brake control, and buck-boost control signals to the turbine board to be optocoupled using turbine power.

Generator Selection

The team decided to use an off-the-shelf brushless DC motor to generate electricity from the rotation of the turbine. Although a brushless motor generates AC, the efficiency loss of a rectifier and filter circuit is less than that of brushes. Additionally, the team did not have the necessary resources and manpower to build a custom generator from scratch. After researching 8 generators, the team decided to use the Maxon EC-i40 488607. Generators were compared using a model that assumed a fixed mechanical power input at

each wind speed and then found a theoretical optimal load for electrical power generation. The model gave estimates for power generation, torque, angular velocity, voltage, and current for each wind speed. The expected power generation at each wind speed was adjusted with tournament weighting and then summed to give a generator score. The Maxon EC-i40 488607 had the second-highest generator score and large factors of safety for maximum angular velocity, torque, voltage, and current predicted by the model. Images of the efficiency curves and power generation for each of the 8 generators are shown in Figure 14.
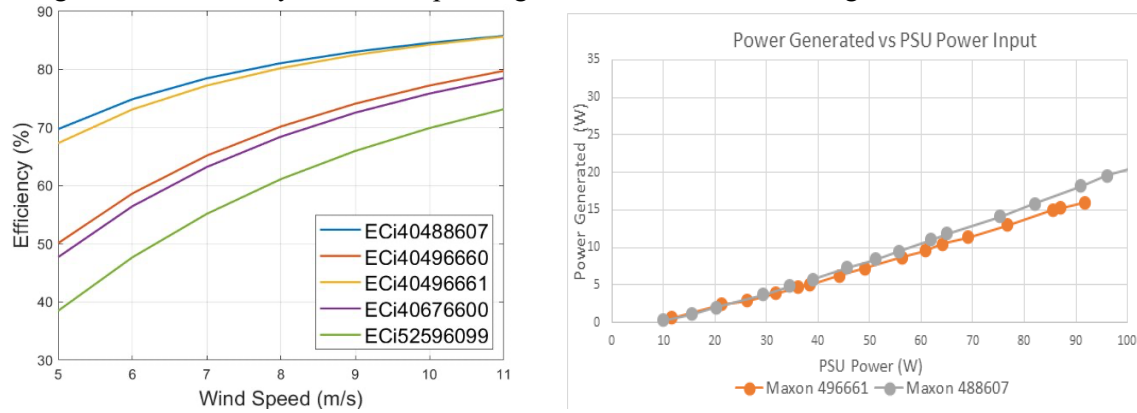

Figure 14. Modeled generator efficiency curves (left) and power generation from testing (right)

To confirm the generator choice, the team produced power curves for 2 generators. To do this, a driving motor was used to spin a shaft connected to the generator being tested and the power output corresponding to each RPM (as measured with a tachometer) was measured. This test was performed on both the Maxon EC-i40 40488607 and 40496661 models, and it was found that the Maxon EC-i40 488607 operated more efficiently leading to its selection in the final turbine design.
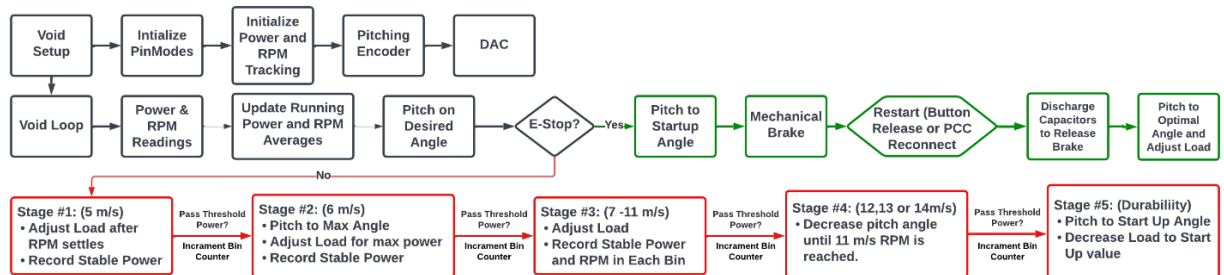
Control States and Operational Modes

Figure 15. Diagram depicting the full turbine control algorithm and stages.

The full turbine control algorithm includes a wide variety of component setups, functions and initializations. This all happens prior to the main algorithm loop which iterates based on E-Stop conditions and sensor readings. In terms of operational modes of the turbine, there are a total of four main stages based on the logistics of the competition testing. Each stage depends on whether an E-Stop condition has been met and the wind speed. The wind speed is determined by a counter sequence based on the power increments determined at each respective speed.

For the first stage from 0-5 m/s, the load resistance will be reduced to assist in startup and the blades will maintain a pitch position for cut-in at low wind speed. We do not predict having enough power to pitch at 5m/s. Once the wind speed increases to 6m/s, our controls allow the rotor to accelerate and once there is enough power to pitch. Then the blades will pitch in increments to a 50° angle, this serves to maximize RPM. The controls algorithm will then incrementally introduce load until maximum power is reached. In the 7-11 m/s bins, the system will only adjust load to maximize power. The maximum stable

12

power and RPM at 11 m/s are saved. For control of rated power and RPM, the rotor is given time to spin to a higher power and RPM than the 11m/s max. Then it will pitch to less aggressive angles until the 11m/s RPM is reached. In the case of an E-Stop condition at any point in these stages, the turbine will revert to optimal startup conditions (pitch and load) and apply the mechanical brake until the turbine reaches a reduction to 10% of its maximum RPMs, as stated in the rules. To automatically restart, the brake will be released with energy from the capacitor bank mentioned above. Then it will pitch to 50° and re-introduce load as per the bin in which e-stop was activated.

Software Architecture

When it comes to the development of the software, the foundation was primarily constructed based on the compatibility of the components with an Arduino Uno. With this, individual control files for each component were generated. Each of these then underwent minimum communications tests to verify their functionality and capabilities. Once full-scale functionality for each component was achieved, we integrated the full system.

To begin with full system integration, the software was developed in a piece-by-piece fashion to verify compatibility on a smaller scale. With this, different variations of compatibility were verified when it came to the load, hall effect sensor, pitching system and braking system. Once these were all verified to be compatible and functional with one another, the software from each component was able to be combined into one final file.

To test this full system integration, the full turbine was then placed into a wind tunnel where it was able to simulate testing conditions expected at competition. From this testing, we then modified the software architecture based on the data findings and generated the respective power increment stages. These modifications allowed for finding proper pitching angles, load resistance values and respective power increments for each respective stage/wind speed.

Regarding data acquisition, the Arduino Uno was utilized in unison with PuTTY to act as a data acquisition machine. When it comes to data recording, the turbine can send data regarding current, voltage and RPM. With these data recordings, functions were then implemented within the full system controls to acquire wind speed and power values.

Final Assembly

The wind turbine was divided into 4 subsystems: the foundation; the structure, comprised of the tower, yaw mechanism; and the nacelle, containing the rotor system (blades and pitching system), the nacelle baseplate, generator mount, pillow blocks supporting the rotor and driveshaft, and emergency brake; and the electrical and controls systems, including the PCBs, harnesses and cabling and control algorithms.

The distributed team environment was managed through ample communication both in-person and online, weekly meetings, and trial and error. Team members chose which subsystem they'd like to work on in the early weeks of the project. Everyone oversaw part of a subsystem, such as blade design, electromechanical integration, and the suction caisson. Maintaining communication between team members was key to ensuring designs could be properly integrated and that a variety of design failure points were considered.

Assembly and Commissioning Checklist

Installation

- Run commissioning code on the nacelle system to set startup pitch angle.
- Run the cables through the top of the foundation and out through the slot. Ensure there is at least 14 inches (0.3556 m) of cable on the tower side, and 106 inches (2.69 m) on the PCC side. Hold ends together to keep dry.
- Install the foundation.
    - Unscrew the three bolts on the foundation so they are engaged with only 1-2 threads.
    - Put the foundation in the water and push it all the way into the sand.
    - Ensure the foundation is level using the provided bubble level.

- o Tighten the three bolts on the foundation using the extended socket wrench.
- Run the cable through the competition stub piece and attach the stub piece to the foundation.
- Place the pre-assembled turbine through the wind tunnel door and attach the cable connectors.
- Tighten stub assembly wing nuts.
- Align the yaw mechanism with the wind direction and tighten the set screws.
- Attach the cables to the PCBs outside of the tunnel.
- Plug the load side into the wall power supply.

Commissioning

- With the tunnel wind speed at 11 m/s, record the power output of the turbine and set this value in the control code to calibrate the control of rated power portion of testing.
- Still at 11 m/s, test that the emergency stop mechanisms will actuate and slow the rotor speed sufficiently under both emergency stop conditions.

Testing

Foundation Stability Test

The foundation stability test procedure involved installing our foundation in the competition-specified sand and water configuration, and ultimately sought to quantify the maximum load that can be applied at the turbine's nacelle before displacing the turbine at the vertical location of the bottom of the wind tunnel by a maximum of 25 mm. The foundation assembly was able to support a maximum load of 66.75 Newtons before displacing 25 mm. To make a conservative estimate of the maximum horizontal force the turbine will experience during competition testing, the power of the wind at 22 m/s was calculated to result in a maximum force of 36 N at the rotor, yielding a factor of safety of 1.89.


Figure 16. Experimental setup of the structural stability test. The foundation is mounted to competition testing specifications in the metal horse trough on the right side of the image.

Emergency Brake Test

To test the functionality of the braking mechanism, a flywheel designed to replicate the expected moment of inertia of the rotor components was attached to a drive train, which was also connected to the disc brake system and a gear that meshed with a driving motor. The driving motor was used to spin the shaft up to maximum speeds of 2200 rpm. The brake was able to bring the system to a full stop in under 2 seconds.
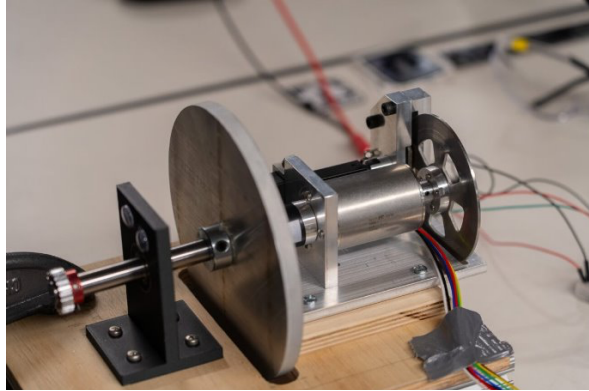
Figure 17. Mechanical brake test setup.

Rotor Spin Test

Mechanical failure is most likely to occur at the rotor, either due to fracture of a blade or failure at the point of interconnection of the blade shaft. Last year's team also reported difficulties with the blades loosening within their blade shafts after repeated testing, so the team would like to see if design modifications have resolved this issue. This testing was particularly important to complete prior to testing in the wind tunnel to ensure there would be no turbine debris that could damage the tunnel or harm the team. We drove the rotor from the generator side of the drive shaft to rotational velocities ranging from 600 to 3200 RPM. Between each test we visually inspected all rotor components. Then we spun the rotor to 3200 RPM and actively pitched 90 degrees. Finally, we spun the rotor at 3200 RPM for 20 minutes. In all cases there was no damage, failure, or signs of fatigue.

Load Test

To ensure our ability to manage and maximize the power being generated by the turbine, we tested the MOSFET load with feedback current control detailed above on a protoboard. We combined a protoboard rectifier and filter with the same driving motor test setup to simulate the wind spinning the generator and set up the current control circuit to be controlled manually through the Arduino IDE serial monitor. The test itself involved externally measuring the current through the load at various generator speeds and various current settings to determine how well the circuit keeps current constant at various RPM and how accurately it could set the current through the load. We found that the regulation worked spectacularly, and the measured current showed very little fluctuation (<1%) with high fluctuations of more than 15 V of input voltage. The accuracy of the current setting against the actual measured current had a margin of error, but this error was very linear, staying constant at about 20 mA difference between the set and measured current. There is only a slight increase in the discrepancy at very low currents and at a very low voltage to current ratio where the op-amp is at max output and the MOSFET is at its minimum resistance. This result gave us confidence in our design since the circuit only needs to be able to regulate current relative to power rather than at an absolute value.

Wind Tunnel System Integration Testing

Previous CU teams have not had access to a competition specification wind tunnel for testing. This year, we have had access to a wind tunnel from the University Corporation for Atmospheric Research (UCAR), and we also have a team of fourth-year mechanical engineering students nearing completion of a wind tunnel on campus that meets CWC testing specifications. So far, wind tunnel testing has been used to integrate the electrical and mechanical systems and simulate the expected conditions of competitions. Data points relating wind speed, load, and pitch angle have helped characterize the expected behavior of the full system, thus informing controls protocols and identifying issues to resolve prior to competition.

References

[1] M. Ragheb, "Optimal Rotor Tip Speed Ratio," Worcester Polytechnic Institute, 2014. [Online]. Available: users.wpi.edu/~cfurlong/me3320/DProject/Ragheb_OptTipSpeedRatio2014.pdf. [Accessed 28 Nov 2023].

[2] B. Nussey, "What can you do with a megawatt-hour?," Accessed: . [Online]. Available: https://www.freeingenergy.com/what-is-a-megawatt-hour-of-electricity-and-what-can-you-do-with-it/. [Accessed 18 Apr. 2024].

[3] P. J. Moriarty and A. C. Hansen, "AeroDyn Theory Manual," *NREL,* 2005.

[4] S. Socket. [Online]. Available: https://www.safetysocket.com/wp-content/themes/epca/files/parts/bd/Products/setscrewtorque.htm .

[5] B. Liu, Y. Zhang, Z. Ma, K. Andersen, H. Jostad, D. Liu and A. Pei, "Design considerations of suction caisson foundations for offshore wind turbines in Southern China," *Applied Ocean Research,* vol. 104, 2020.

[6] National Renewable Energy Laboratory (NREL), [Online]. Available: https://wrdb.nrel.gov/data-viewer.

[7] N. R. E. L. (NREL). [Online]. Available: https://wrdb.nrel.gov/data-viewer.

[8] W. D. e. a. Pilkey, Peterson's Stress Concentration Factors, Wiley, 2020.